NASA Technical Memorandum 102332

Fatigue Crack Growth Study of SCS_6/Ti-15-3 Composite

Peter Kantzos and Jack Telesman
Lewis Research Center
Cleveland, Ohio

August 1989

NASA

FATIGUE CRACK GROWTH STUDY OF SCS_6/Ti-15-3 COMPOSITE

Peter Kantzos and Jack Telesman
National Aeronautics and Space Administration
Lewis Research Center
Cleveland, Ohio 44135

SUMMARY

A study was performed to determine the FCG behavior and the associated fatigue damage processes in a $[0]_8$ and $[90]_8$ oriented SCS6/Ti-15-3 composite. Companion testing was also done on identically processed Ti-15-3 unreinforced material.

The active fatigue crack growth failure processes were very similar for both composite orientations tested. For both orientations, fatigue crack growth was along the fiber direction. It was found that the composite constituent most susceptible to fatigue damage was the interface region and in particular the carbon coating surrounding the fiber. The failure of the interface region lead to crack initiation and also strongly influenced the fatigue crack growth (FCG) behavior in this composite. The failure of the interface region was apparently driven by normal stresses perpendicular to the fiber direction.

The FCG rates were considerably higher for the $[90]_8$ oriented CT specimens in comparison to the unreinforced material. This is consistent with the scenario in which the interface has lower fatigue resistance than the matrix, causing lower composite fatigue resistance. The FCG rates of the $[0]_8$ composite could not be directly compared to the $[90]_8$ composite but were shown to increase with an increase in the crack length.

INTRODUCTION

The new generation of the aerospace vehicles will require materials capable of withstanding high temperatures while retaining a high stiffness under relatively high loads. Continuous fiber, metal matrix composites (MMC) are candidate materials for such applications. One of these candidate materials consisting of a Ti-15V-3Cr-3Al-3Sn matrix reinforced by continuous, unidirectional SiC fibers, was investigated.

The fatigue behavior and life prediction of MMC's must be understood before they can be widely utilized in aerospace applications. However, relatively little information is available concerning the fatigue behavior of continuous fiber reinforced composites. The objective of this study has been to determine the microstructural processes controlling fatigue crack initiation and propagation in this system. Emphasis has been placed on the identification of the composite constituent most susceptible to fatigue damage.

MATERIAL

The composite used in this study is a Ti-15V-3Cr-3Al-3Sn (Ti-15-3) alloy matrix reinforced by 145 μm average diameter, continuous SiC (SCS_6) fibers. All the composite specimens used in this study were obtained from a single,

eight-ply, unidirectional panel manufactured by Textron Specialty Materials Division. The panel size was 30 by 30 by 0.21 cm. Also tested were specimens machined out of a 30- by 30- by 1-cm panel made without fibers, using the same Ti-15-3 foil and same consolidation techniques employed in composite production.

The matrix is a metastable beta phase alloy, chosen because it can be cold rolled to very thin sheets. This enables a more cost effective processing of the composite. Sample micrographs of both, the unreinforced and reinforced composite are shown in figures 1 and 2. The SiC fiber is surrounded by a complex multilayer structure (fig. 2(b)) which consists mainly of a multilayer carbon coating approximately 3 μm thick and an approximately 0.5-1 μm thick reaction zone consisting mainly of brittle intermetallic phases (ref. 1). The combination of the carbon layers and the reaction zone will henceforth be referred to as the interface region.

HEAT TREATMENT

Specimens were tested both in the as-received and heat treated condition. The heat treatment consisted of 24 hr at 700 °C in vacuum. The purpose of the heat treatment was to precipitate out most of the alpha phase. The heat treatment did not produce any additional noticeable fiber/matrix interactions and the reaction zone remained unchanged (ref. 2).

MECHANICAL TESTING

Testing was performed using compact tension (CT) specimens, such as the one shown in figure 3. The specimens were tested in two orientations: (1) longitudinal, $[0]_8$, with fibers oriented parallel to the loading direction; and (2) transverse, $[90]_8$, with fibers perpendicular to the loading direction.

All machining was done using diamond tip tools. Prior to testing, all specimens were polished to enhance crack detection. The polishing process was automated and developed at NASA Lewis Research Center (ref. 3).

The test matrix is shown in table I. Testing of the CT specimens was performed at room temperature and ambient environment using a computer controlled, closed loop, servohydraulic machine. The tests were performed using constant load range at a frequency of 5 Hz and $R = 0.5$. The crack length was obtained by measuring compliance of the specimen through a clip gage mounted in the crack mouth of the specimen. Data was also gathered through periodical optical readings to ensure accurate results.

POST-FAILURE ANALYSIS

Following each test, extensive metallography and fractography was performed in order to evaluate fatigue failure processes. Each sample fracture surface was examined in the scanning electron microscope, with some samples also being sectioned to determine the extent of damage.

RESULTS

Longitudinal, $[0]_8$ Specimens

The overall direction of fatigue failure for $[0]_8$ oriented specimens was parallel to the loading direction and perpendicular to the machined notch, as shown in figure 4. The fatigue crack growth (FCG) data for the $[0]_8$ specimens is shown in figure 5 in the form of crack length a versus number of cycles N (fig. 5(a)) and crack growth rate da/dN versus a (fig. 5(b)). The data was not analyzed in terms of the applied ΔK due to the lack of K_I and K_{II} solutions for a crack in a CT specimen growing parallel to the loading direction. The FCG data, shown in figure 5, does reveal an increase of the FCG rate with an increase in the crack length indicating a probable increase of the crack tip stress field with crack growth.

A fractographic evaluation was performed to reveal the fatigue failure processes which resulted in this rather unusual behavior. The first row of fibers at the machined notch were partly damaged by the machining process (fig. 6). The damaged fibers at the notch produced multiple crack initiations at the fiber/matrix interface regions. Upon further fatigue loading, these small interface cracks propagated into the matrix ligaments and joined (fig. 7(a)). When the coalesced cracks encountered the next row of fibers, the crack trajectory changed and the cracks started growing along the fiber direction as shown in figure 6. In these early stages of fatigue life there appears to be an extensive amount of microcracking and crack coalescence (fig. 7(a)). In the later stages of the fatigue life, the microcracks coalesced to form one dominant crack. Once this crack formed, the damage appears to be mostly confined to the main crack front with little evidence of secondary cracking (fig. 7(b)). After the dominant crack reached a critical length, the specimens failed through debonding of the fibers and tearing of the matrix.

The microcracking appears to have initiated typically in the fiber/matrix interface region. The crack initiation sites were not evenly distributed with an observed preference for initiation to occur in a thickness direction (fig. 7(a)). A closer examination revealed a somewhat greater tendency for the cracks to initiate in the carbon coating of the fibers (fig. 8(a)) rather than the reaction zone adjacent to the coating. As shown in figure 8(a), crack initiated between the carbon coating layers, cracked through the reaction zone and entered the matrix (crack width in the matrix is exaggerated due to the preferential etching of the/matrix material adjacent to the crack). Irregardless of the precise crack initiation location, the microcracks usually tended to encompass both the carbon coating as well as the brittle intermetallic reaction zone (i.e., the entire interface region). Post failure analysis revealed suspected carbon coating regions adhering to the matrix after the fiber has broken away, again indicating that cracking must have occurred between the fiber and the coating (fig. 8(b)). These results support recent findings of Gabb et al. (4) who also identified the carbon coating as a site for preferential crack initiation. Johnson et al. (5) while not differentiating between the carbon layer and the reaction zone, also noted that the weak interface region is responsible for degradation of fatigue life of this composite.

Post failure fractographic analysis revealed that the interface region was not only the site for preferential crack initiation but was also the controlling factor which influenced crack propagation behavior. Throughout the entire test the crack growth occurred preferentially in the interface region. The

crack growth process consisted of the continuous cracking of the interface region at or ahead of the crack tip, followed by crack growth into the matrix ligaments and crack coalescence. This phenomena is illustrated in figure 9. In particular, note in the fractograph (fig. 9(b)) of a high da/dN region just prior to final failure, that stable crack growth has occurred in the areas adjacent to the interface. However, the remaining part of the matrix ligament failed through void coalescence during the catastrophic failure. This fractograph clearly shows the direction of localized crack growth to be from the interface region to the matrix ligament.

The crack propagation within the matrix was transgranular in nature (fig. 9). The active fatigue failure mechanisms in the matrix were dependent on grain orientation, and included evidence of striation formation, slip decohesion and/some cleavage. Some secondary cracking was present in the matrix foil laminate boundaries perpendicular to the main crack front.

Transverse Composite, $[90]_8$, and Unreinforced Matrix Material

Contrary to the behavior of the $[0]_8$ specimens, for both the $[90]_8$ composite and the unreinforced matrix material the crack growth direction was perpendicular to the applied load. The comparison of the FCG behavior for the two materials is shown in figure 10. As shown for the ΔK range tested, the crack growth rates for the $[90]_8$ oriented composite are always considerably higher than those of the unreinforced material. Possible reasons for this type of behavior will be discussed later.

The FCG data in figure 10 is shown for both the heat treated and as-received conditions. For the limited number of tests conducted, there appears to be no appreciable effect of heat treatment on the FCG behavior of the unreinforced material. However, in the $[90]_8$ composite the heat treated material exhibits higher FCG rates in the high ΔK region.

There were many similarities between the FCG processes observed for the $[90]_8$ specimens and those already described for the $[0]_8$ specimens. For the $[90]_8$ oriented composite, just as in the $[0]_8$, the crack initiation occurred mostly in the fiber/matrix interface regions of fibers damaged by the machining process. Figure 11 shows a notch area where the fibers have pulled away from the matrix, leaving in its wake portions of the carbon coating. This indicates that crack growth was accompanied by the cracking of the carbon coating. In a manner very similar to the $[0]_8$ oriented material, crack growth occurred preferentially in the interface region, followed by growth into the matrix ligaments (fig. 12). Again, the matrix deformed mainly by slip decohesion and striation forming mechanisms. In the final stages of cracking, the same mechanisms of debonding and matrix tearing were observed as in the $[0]_8$ specimens. There were no major differences in the failure processes between the heat treated and as-received composite.

The fatigue failure in the unreinforced matrix material tended to be mostly transgranular and consisted mostly of slip decohesion and striation forming mechanisms in the stable crack growth region. Some intergranular failure and void coalescence occurred in the high ΔK and overload regions. The fatigue failure processes were thus usually similar to those encountered in the composite material.

The unreinforced matrix material exhibited some delamination at the foil boundaries (fig. 13). Delamination can be attributed to the poor bonding during consolidation caused by the presence of contaminants at the foil boundaries. Delamination increased with an increase in the applied ΔK.

DISCUSSION

One of the major findings of the study was the close similarity of the fatigue failure processes for the two different composite orientations (compare figs. 9 and 12). The most important event which lead to this similarity in the fatigue behavior was the preferential cracking of the interface region, in particular the carbon coatings surrounding the fibers. The cracking of the interface region occurred for both orientations tested, and promoted crack growth being confined to the fiber direction. While crack growth in the fiber direction is not to surprising in the $[90]_8$ oriented specimens, it is somewhat surprising in the $[0]_8$ specimens. For the $[90]_8$ specimens, cracking of the weak interface region normal to the applied tensile load apparently occurred first. These microcracks later propagated into the matrix and linked up resulting in a dominant crack growing in the fiber direction. For the $[0]_8$ specimens, with the main crack growing in the direction of the applied load, one would expect the shear stresses to control the FCG behavior. However, calculations of the simple shear and bending stresses, shown in table II and figure 14, reveal that the bending stress σ_{xx} perpendicular to the fiber direction, is initially twice that of the shear stress τ_{xy} parallel to the fibers, with the ratio increasing as the crack grows further in the fiber direction. These relatively high bending stresses must have been high enough to initiate cracking of the interface region perpendicular to the σ_{xx} direction (fig. 7(a)). The cracking in the interface region was followed by propagation and linkage of the cracks in the matrix ligaments. The relatively high shear stresses in the $[0]_8$ specimens might have further contributed to keeping the crack front in the fiber direction by weakening the fiber/matrix interface. However, from the fractographic evidence, as well as the above mentioned analysis, it appears that tensile loads perpendicular to the fiber direction played the major role in controlling the FCG behavior of this composite system by preferentially cracking the interface region.

A schematic illustration of the crack initiation and propagation processes discussed above, for both composite orientations, is proposed and shown in figure 13. The process can be summarized as follows: (1) cracking of the interface region perpendicular to the applied tensile loads; (2) local debonding occurring in the failed interface region and growth of microcracks into the matrix; (3) linking of the cracks in the matrix ligaments. This is a continuing process requiring continuous cracking of the interface region layer at or ahead of the crack front.

The FCG rate of the $[90]_8$ composite was considerably greater than that of the unreinforced matrix for a given stress intensity tested (fig. 10). The fatigue mechanisms within the matrix region (i.e., slip decohesion, formation of striations, etc.) were very similar for both the $[90]_8$ and the unreinforced material and thus probably did not contribute to the observed differences in the FCG rates. However, the ease of cracking of the interface region, in particular the carbon coating, is probably responsible for the increase in the crack growth rates. This is consistent with the hypothesis that the fiber/

matrix interface has lower fatigue resistance than the matrix. This weak composite constituent therefore limited the fatigue cracking resistance of the composite.

CONCLUSIONS

A study was performed to determine the FCG behavior and the associated fatigue damage processes in a $[0]_8$ and $[90]_8$ oriented SCS6/Ti-15-3 composite. Companion testing was also done on identically processed Ti-15-3 unreinforced material. The most important findings were:

1. The fatigue crack growth processes were very similar for the two composite orientations tested, with fatigue crack growth being confined along the fiber direction.

2. The interface region (in particular the carbon coating) was the composite constituent most susceptible to fatigue damage influencing both the crack initiation and crack propagation behavior of the composite.

3. The failure of the interface region was mostly the result of the applied bending stresses perpendicular to the fiber direction.

4. The FCG rates were considerably higher for the $[90]_8$ oriented CT specimens in comparison to the unreinforced material, reaffirming the lower fatigue resistance of the fiber/matrix interface in comparison to the matrix.

REFERENCES

1. Rhodes, C.G.; and Spurling, R.A.: Fiber-Matrix Reaction Zone Growth Kinetics is SiC-Reinforced Ti-6Al-4V as Studied by Transmission Electron Microscopy. Recent Advances in Composites in the United States and Japan, J.R. Vinson and M. Taya, eds., ASTM, Philadelphia, 1985, pp. 585-599.

2. Lerch, B.A.; Gabb, T.P.; and MacKay, R.A.: A Heat Treatment Study of the SiC/Ti-15-3 Composite System. NASA TM (to be published), 1989.

3. Lerch, B.A.; Hull D.R.; and Leonhardt, T.A.: As-Received Microstructure of a SiC/Ti-15-3 Composite. NASA TM-100938, 1988.

4. Gabb, T.P.; Gayda, J.; and Mackay R.A.: Isothermal and Nonisothermal Fatigue Behavior of a Metal Matrix Composite. Submitted to the J. Compos. Mater., 1989.

5. Johnson, W.S., et al.: Mechanical Characterization of SCS_6/Ti-15-3 Metal Matrix Composite at Room Temperature. NASP TM-1014, 1988.

TABLE I. - TEST MATRIX

Material tested	Specimens tested	
	As-received	Heat treated
Longitudinal, $[0]_8$	2	1
Transverse, $[90]_8$	1	1
Unreinforced matrix	1	1

TABLE II. - A COMPARISON OF BENDING AND SHEAR STRESSES FOR THE $[0]_8$ SPECIMENS AT INITIATION AND FAILURE

	Maximum bending stress, MPa	Maximum shear stress, MPa
Initiation	90	45
Failure	220	65

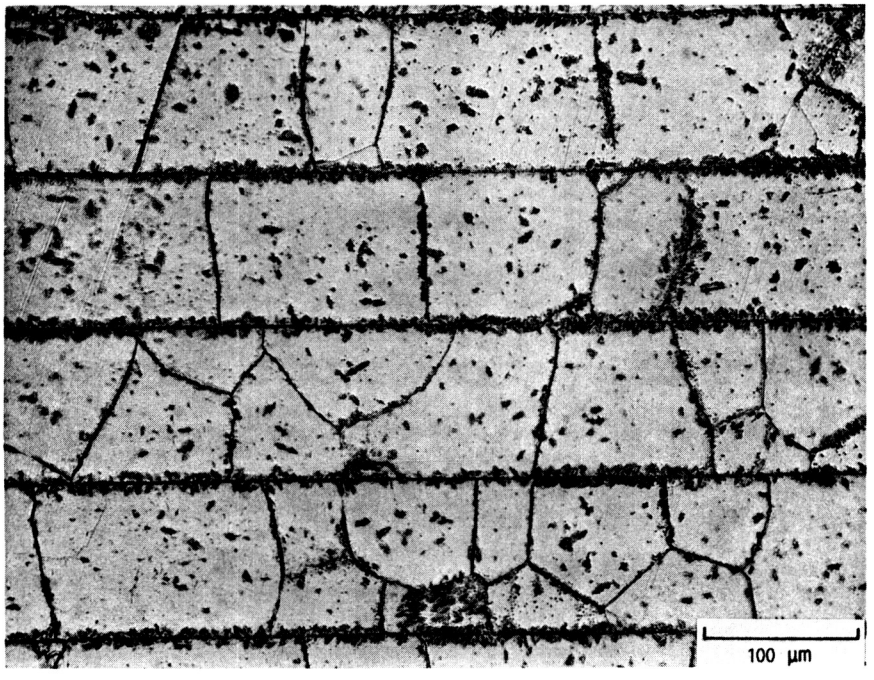

FIGURE 1. - MICROSTRUCTURE OF THE UNREINFORCED MATRIX MATERIAL.

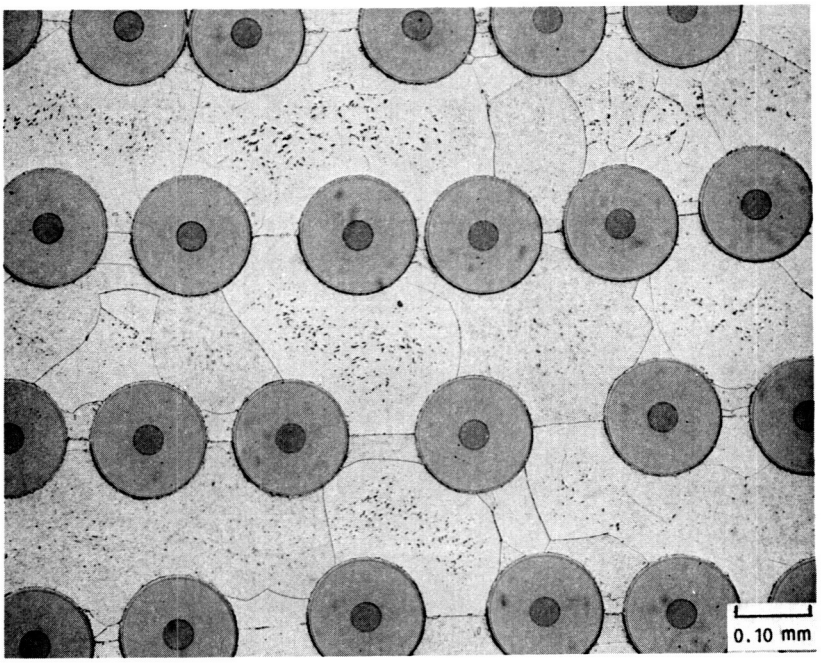

(a) GENERAL MICROSTRUCTURE.

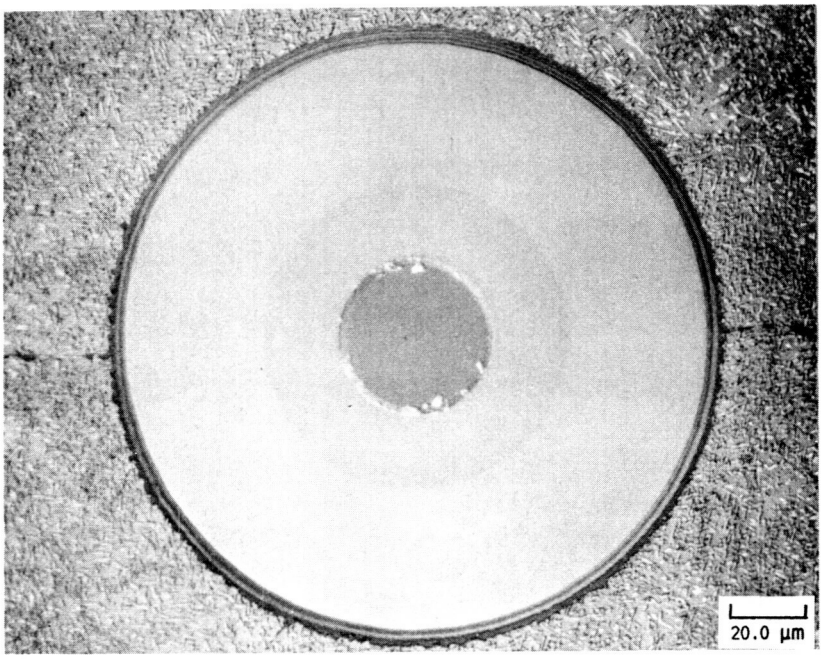

(b) SCS_6 FIBER.

FIGURE 2. - AS RECEIVED COMPOSITE.

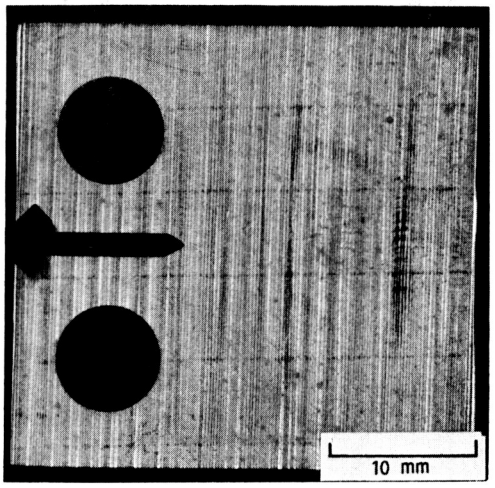

FIGURE 3. - COMPACT TENSION (CT) SPECIMEN.

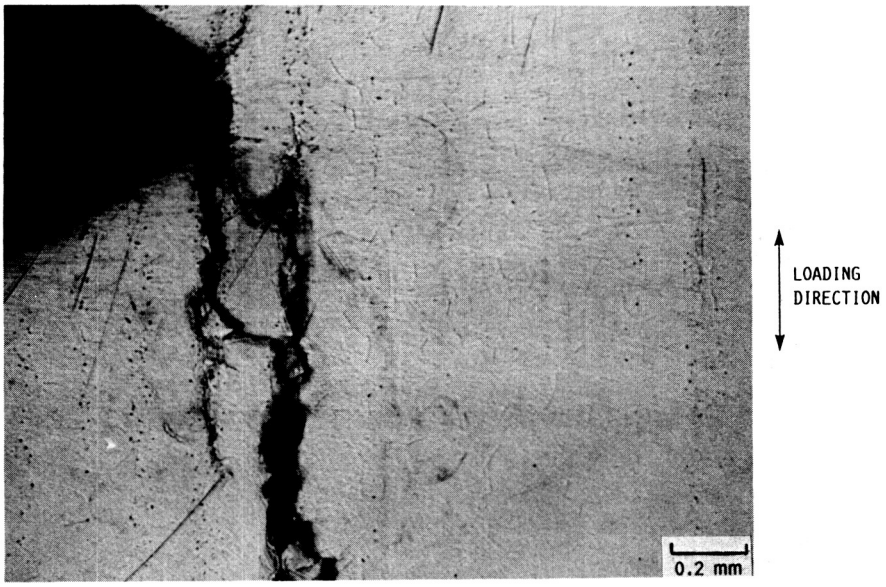

$[0]_8$ ORIENTATION.

FIGURE 4. - CRACK GROWTH PARALLEL TO THE LOADING DIRECTION FOR THE $[0]_8$ ORIENTATION.

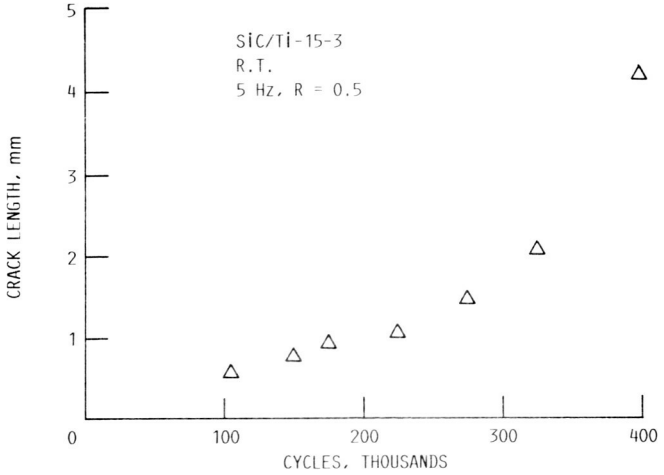

(a) CRACK LENGTH VERSUS CYCLES.

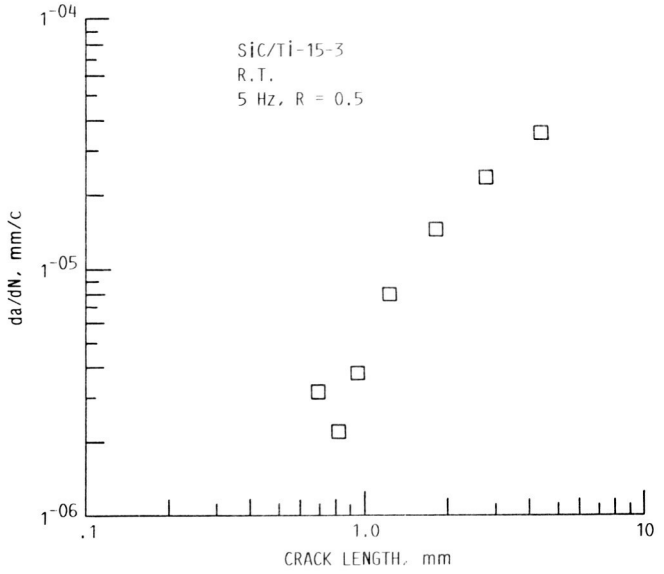

(b) CRACK GROWTH RATE VERSUS CRACK LENGTH.

FIGURE 5. - FATIGUE CRACK GROWTH RATE DATA FOR $[0]_8$ SPECIMENS.

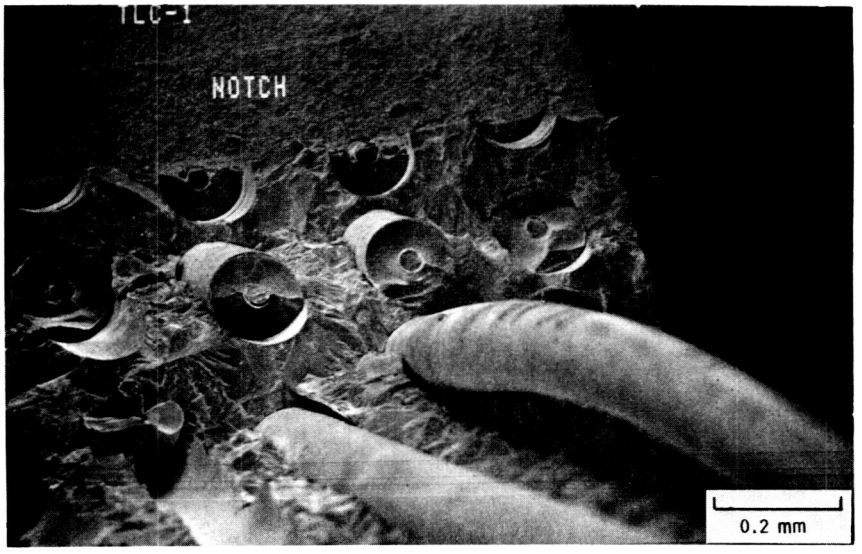

FIGURE 6. - CRACK GROWTH IN THE $[0]_8$ MATERIAL. DIRECTION OF LOADING PARALLEL TO FIBER DIRECTION.

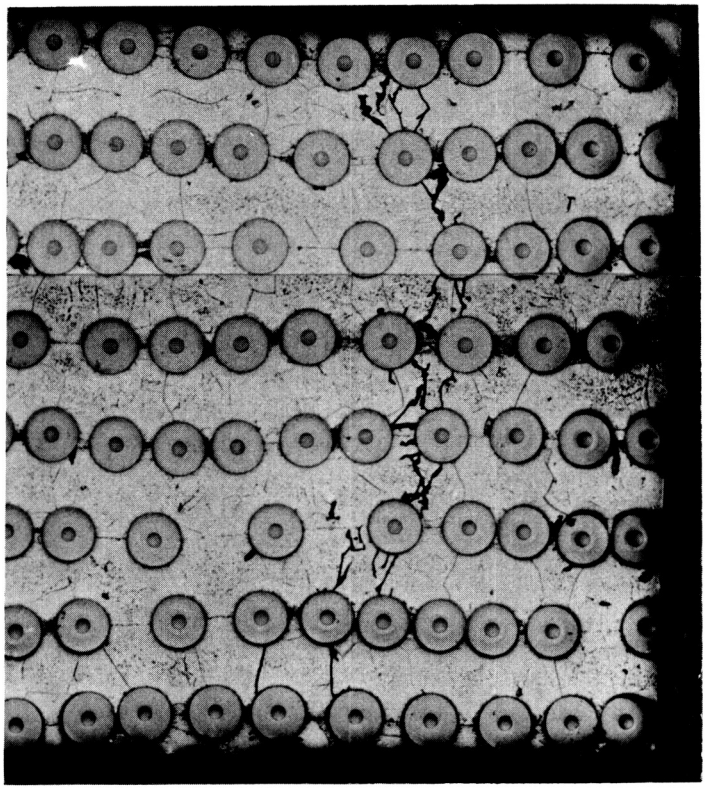

CUT 1

(a) MULTIPLE CRACK INITIATION AND COALESCENCE IN THE EARLY STAGES OF FATIGUE LIFE.

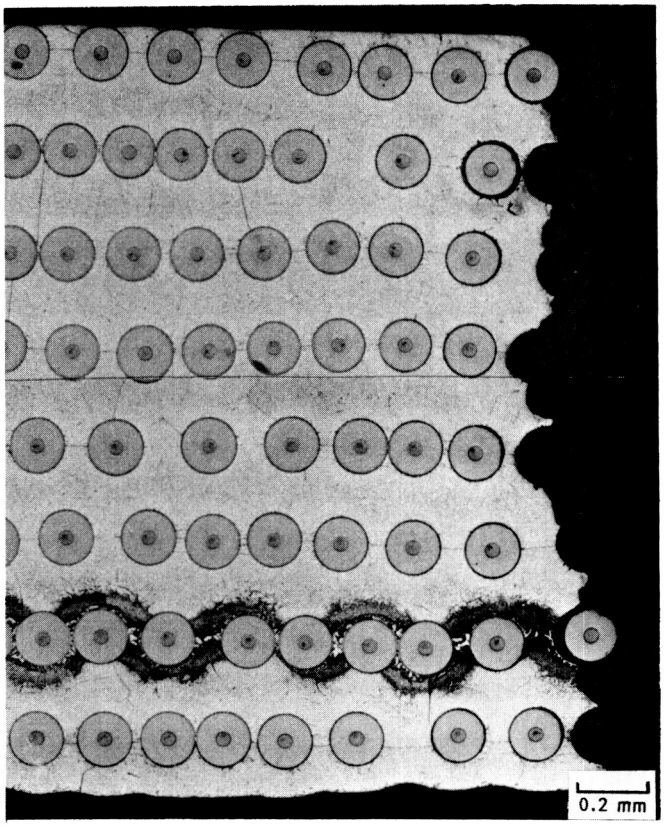

CUT 2

(b) CRACK GROWTH CONFINED MOSTLY TO ONE DOMINANT FRONT IN THE LATER STAGES OF FATIGUE LIFE.

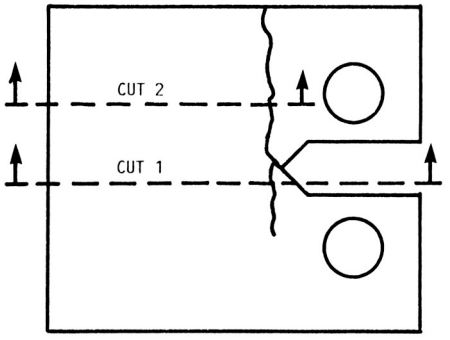

FIGURE 7. - COMPARISON OF EXTENT OF MICROCRACKING IN DIFFERENT STAGES OF FATIGUE LIFE IN THE $[0]_8$ ORIENTED COMPOSITE.

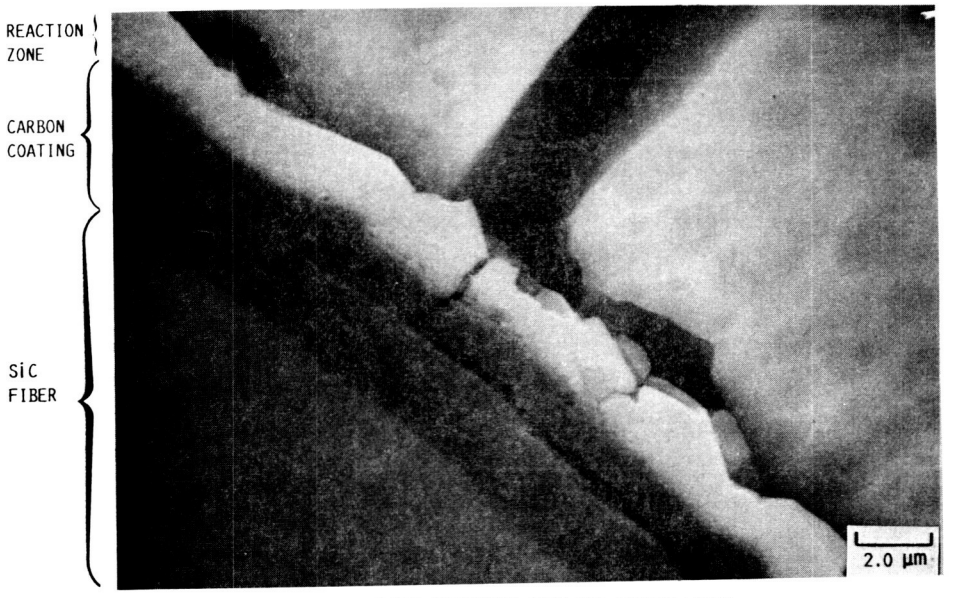

(a) CRACKING EMANATING FROM THE CARBON LAYER.

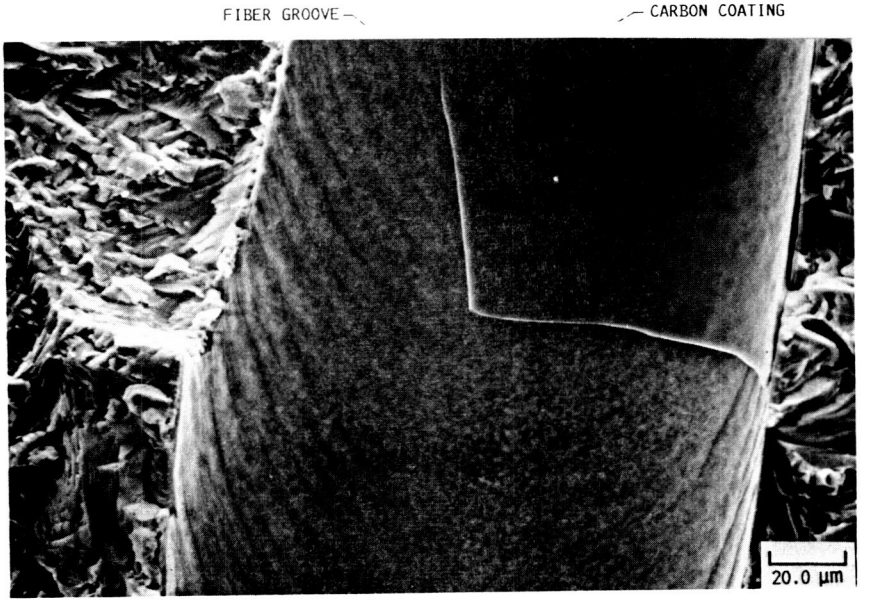

(b) CARBON LAYER SEPARATED FROM THE FIBER DURING FATIGUE.

FIGURE 8. - PREFERENTIAL CRACKING OF THE CARBON LAYER.

(a) LOW da/dN $[0]_8$.

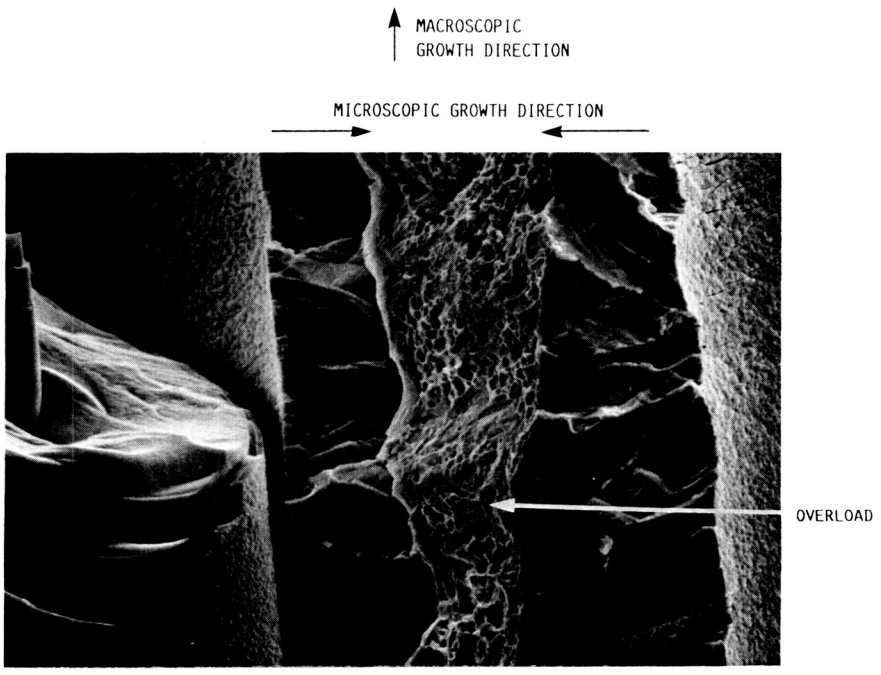

(b) HIGH da/dN $[0]_8$.

FIGURE 9. - MICROSCOPIC CRACK GROWTH DIRECTION FROM THE INTERFACE INTO THE MATRIX LIGAMENT IN THE $[0]_8$ SPECIMENS.

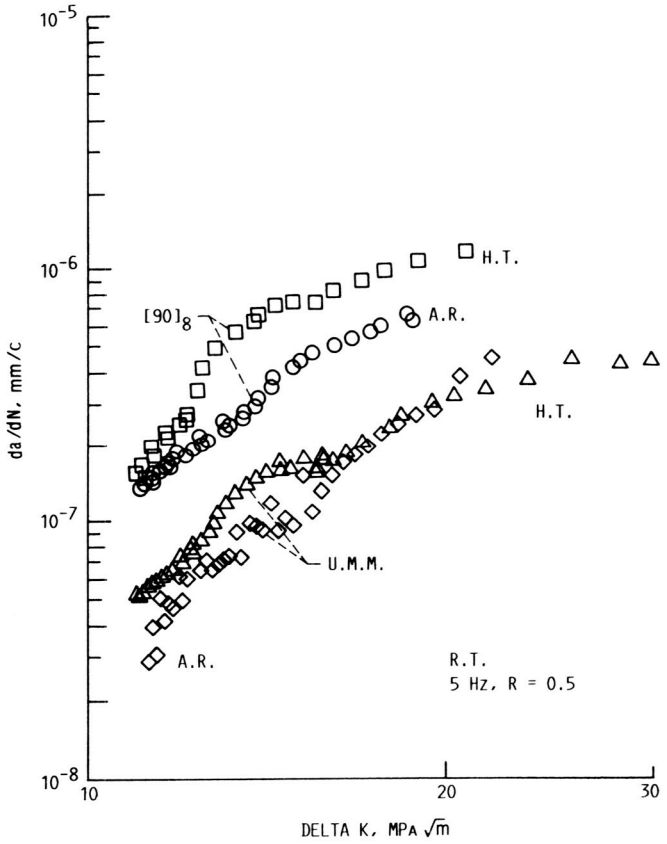

FIGURE 10. - COMPARISON OF FCG RATES FOR THE $[90]_8$ AND THE UNREINFORCED MATRIX MATERIAL IN THE AS-RECEIVED (A.R.) AND HEAT-TREATED (H.T.) CONDITION.

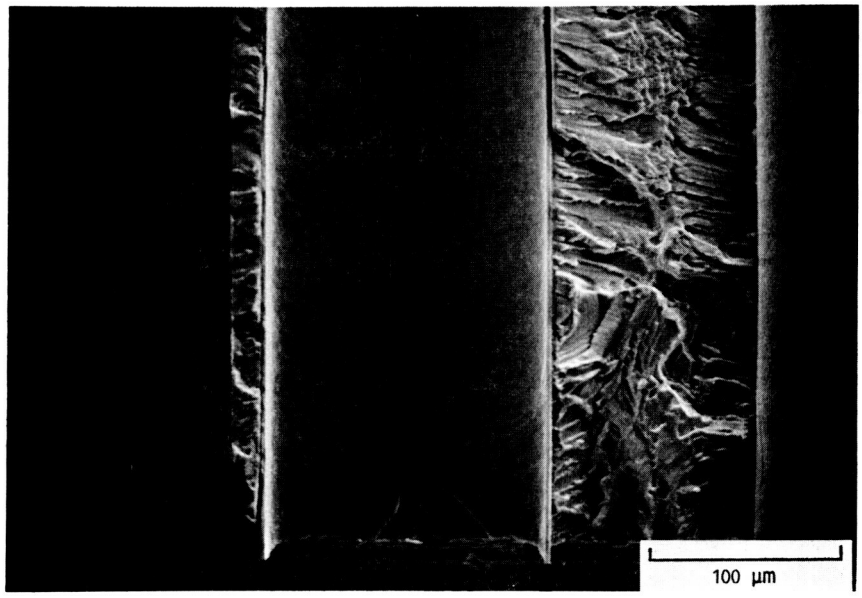

(a) REMNANTS OF THE CARBON COATING ADHERING TO THE MATRIX AFTER ITS SEPARATION FROM THE FIBER IN THE $[90]_8$ COMPOSITE.

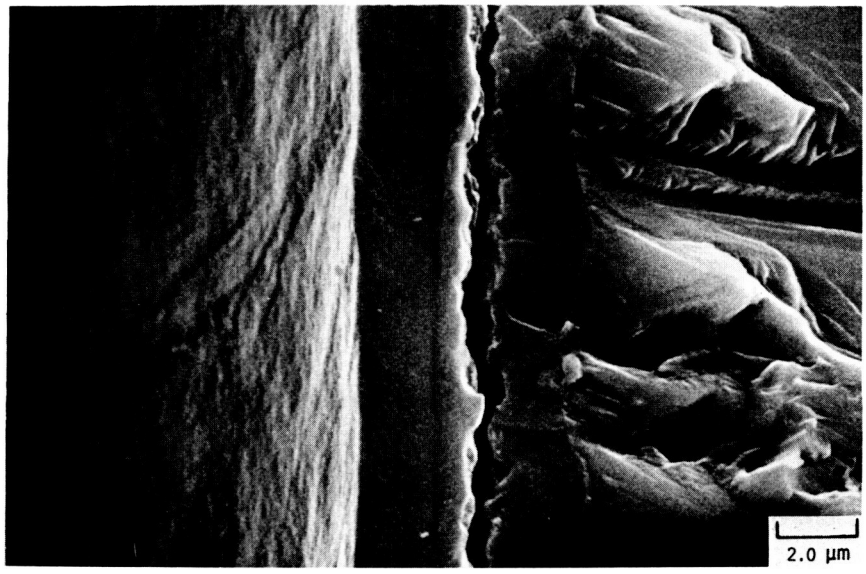

(b) CARBON COATING REMAINING IN THE FIBER GROOVE. IN THE CENTER OF THE FRACTOGRAPH NOTE A CRACK BETWEEN CARBON COATING AND THE INTERFACE.

FIGURE 11. - SEPARATION OF THE CARBON COATING FROM THE FIBER IN THE $[90]_8$ SPECIMENS.

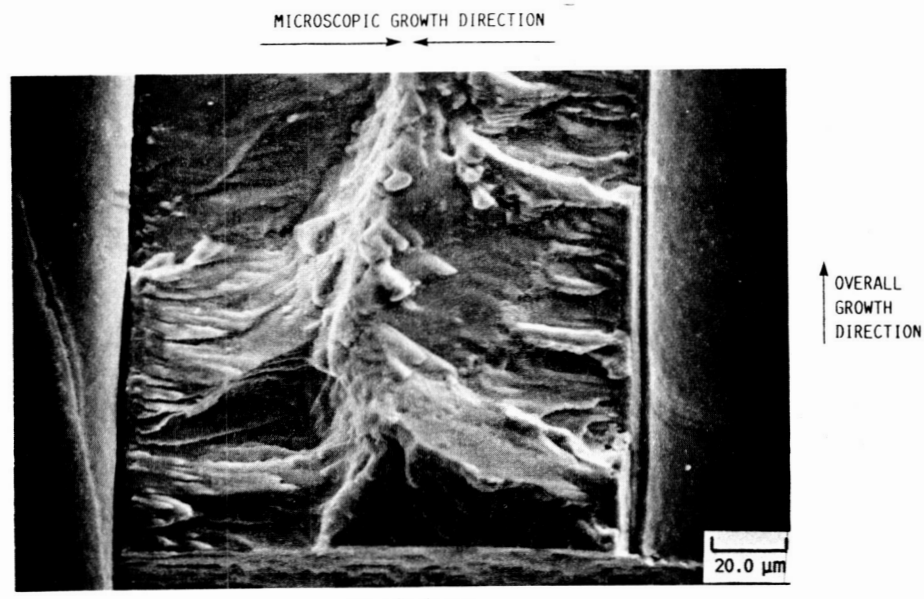

(a) LOW da/dN.

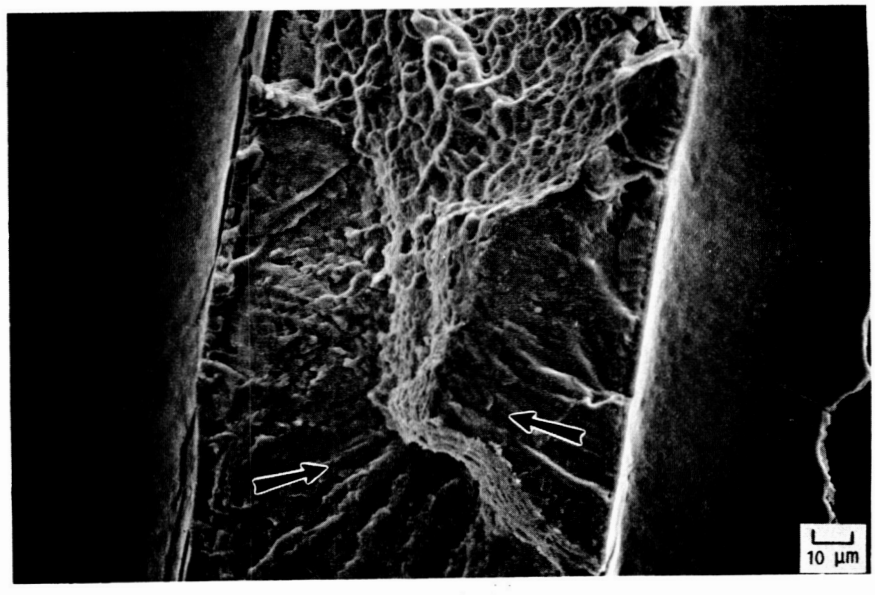

(b) HIGH da/dN.

FIGURE 12. - MICROSCOPIC CRACK GROWTH FROM THE INTERFACE INTO THE MATRIX LIGAMENTS IN THE $[90]_8$ SPECIMENS.

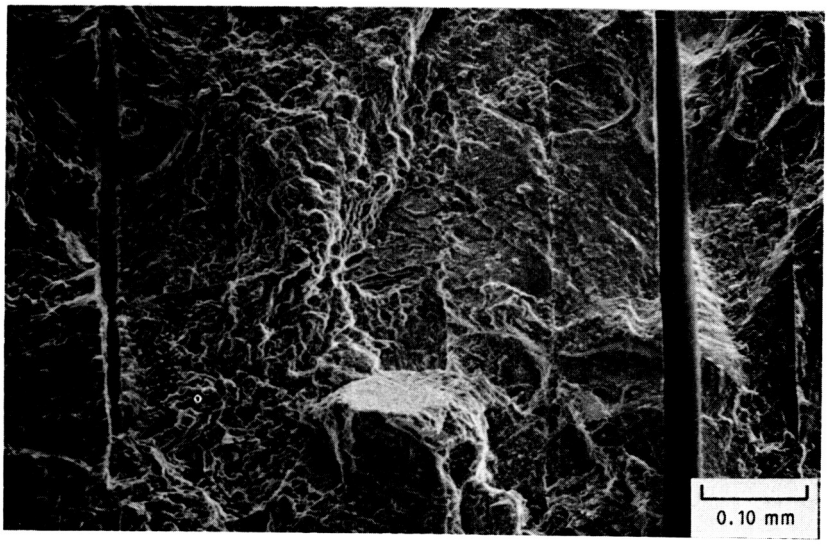

LOW ΔK

(a) SOME PLY DELAMINATION.

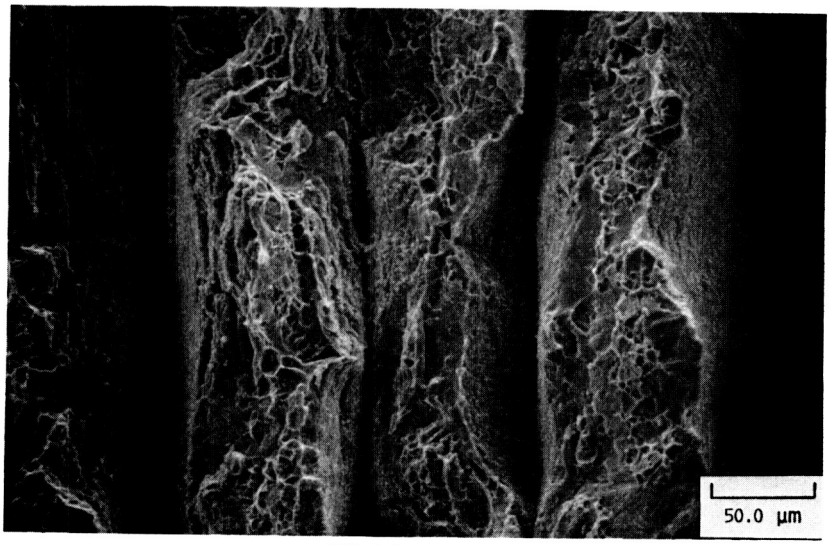

OVERLOAD - HIGH ΔK

(b) EXTENSIVE PLY DELAMINATION.

FIGURE 13. - DELAMINATION IN THE UNREINFORCED MATRIX MATERIAL.

INITIAL K = 18 MPA $\sqrt{m}$
MAXIMUM BENDING STRESS σ_{xx} = 90 MPA
SHEAR STRESS τ_{xy} = 45 MPA

•CRACKING IN THE SPECIMEN PARALLEL TO THE LOADING DIRECTION

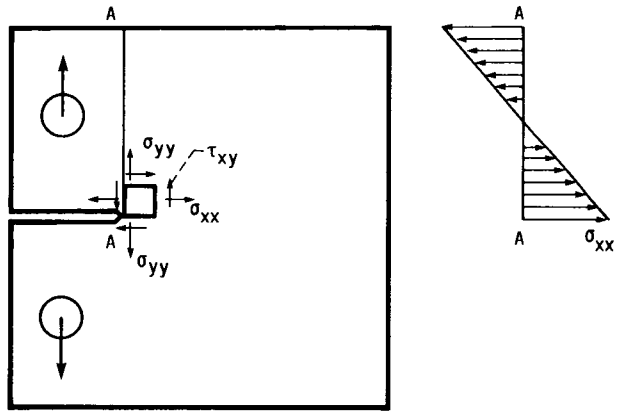

FIGURE 14. - DIRECTION AND MAGNITUDE OF THE BENDING AND SHEAR STRESSES FOR THE $[0]_8$ SPECIMENS AT THE NOTCH.

1 σ_{yy} FOR $[90]_8$ SPECIMENS
2 $\tau_{xy} \cong 0$ FOR $[90]_8$ SPECIMENS

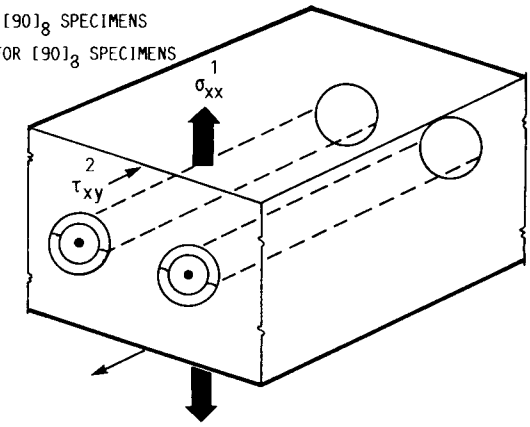

(a) CRACK INITIATION IN THE INTERFACE.

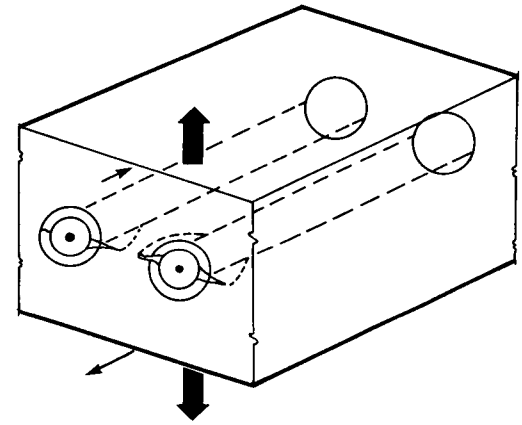

(b) CRACK GROWTH AND LOCAL DEBONDING.

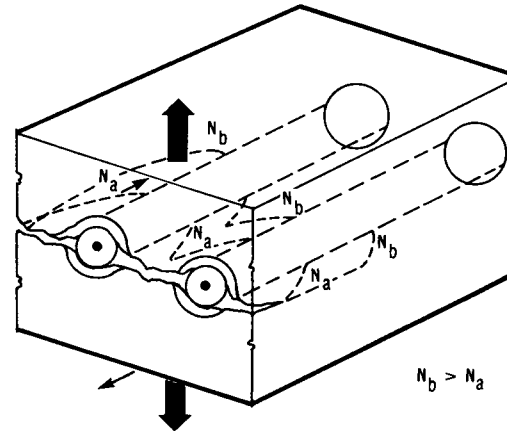

(c) CRACK COALESCENCE IN THE MATRIX.

FIGURE 15. - POSTULATED CRACK INITIATION AND GROWTH SEQUENCE FOR SiC/Ti-15-3 COMPOSITE.

NASA
National Aeronautics and Space Administration

Report Documentation Page

1. Report No.	2. Government Accession No.	3. Recipient's Catalog No.
NASA TM-102332		

4. Title and Subtitle	5. Report Date
Fatigue Crack Growth Study of SCS_6/Ti-15-3 Composite	August 1989
	6. Performing Organization Code

7. Author(s)	8. Performing Organization Report No.
Peter Kantzos and Jack Telesman	E-5041
	10. Work Unit No. 510-01-01

9. Performing Organization Name and Address	11. Contract or Grant No.
National Aeronautics and Space Administration Lewis Research Center Cleveland, Ohio 44135-3191	
	13. Type of Report and Period Covered Technical Memorandum
12. Sponsoring Agency Name and Address	14. Sponsoring Agency Code
National Aeronautics and Space Administration Washington, D.C. 20546-0001	

15. Supplementary Notes

16. Abstract

A study was performed to determine the FCG behavior and the associated fatigue damage processes in a $[0]_8$ and $[90]_8$ oriented SCS_6/Ti-15-3 composite. Companion testing was also done on identically processed Ti-15-3 unreinforced material. The active fatigue crack growth failure processes were very similar for both composite orientations tested. For both orientations, fatigue crack growth was along the fiber direction. It was found that the composite constituent most susceptible to fatigue damage was the interface region and in particular the carbon coating surrounding the fiber. The failure of the interface region lead to crack initiation and also strongly influenced the fatigue crack growth (FCG) behavior in this composite. The failure of the interface region was apparently driven by normal stresses perpendicular to the fiber direction. The FCG rates were considerably higher for the $[90]_8$ oriented CT specimens in comparison to the unreinforced material. This is consistent with the scenario in which the interface has lower fatigue resistance than the matrix, causing lower composite fatigue resistance. The FCG rates of the $[0]_8$ composite could not be directly compared to the $[90]_8$ composite but were shown to increase with an increase in the crack length.

17. Key Words (Suggested by Author(s))	18. Distribution Statement
Metal matrix composite Fatigue Crack initiation Crack propagation	Unclassified – Unlimited Subject Category 26

19. Security Classif. (of this report)	20. Security Classif. (of this page)	21. No of pages	22. Price*
Unclassified	Unclassified	20	A03

NASA FORM 1626 OCT 86

*For sale by the National Technical Information Service, Springfield, Virginia 22161